IMS

INSTITUTE OF MATERIALS SCIENCE

THE UNIVERSITY OF CONNECTICUT

Storrs · Connecticut

INVESTIGATION OF SOLIDIFICATION IN ZERO-GRAVITY ENVIRONMENT; M553 SPHERE FORMING EXPERIMENT

PHASE C REPORT-EVALUATION OF SKYLAB SPECIMENS

CONTRACT NAS8-28734
PERIOD COVERED: MAY 15,1972 - DECEMBER 15,1973

DECEMBER 4,1973

PREPARED FOR

NASA,GEORGE C. MARSHALL SPACE FLIGHT CENTER
MARSHALL SPACE FLIGHT CENTER,ALABAMA 35812

by

Theo Z. Kattamis

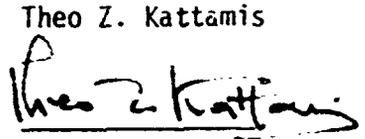

Department of Metallurgy
Institute of Materials Science
University of Connecticut
Storrs,Connecticut 06268

EVALUATION OF SKYLAB SPACIMENS

INTRODUCTION

Results on specimen evaluation and discussion of solidification behavior in each case are reported herein in the following order: specimen SL-1.6,specimen SL-2.8,specimen SL-2.4,specimen SL-1.10 and specimen SL-1.11. Comparison is made with ground-processed specimens of similar composition,whenever pertinent and meaningful.

Among the nondestructive evaluation methods the measurement of sphericity was conducted by micrometric and shadowgraphic techniques. The intricate shape of specimens in some cases appeared difficult to define. In measuring the density,liquid penetration insi_ cavities that outcrop on the surface was avoided by sealing off these cavities.

Among the destructive evaluation methods the use of the Quantimet 720 required particular attention,because of the small difference in contrast between second phases and micropores. With regard to microporosity microvoids in the core of some specimens were so fine that X-ray microradiography had to be used. Quantitative results from application of this method had to be interpreted with caution,because of the small areas covered at high magnification. The identification of individual nonmetallic inclusions and the evaluation of their volume percent and average ize was conducted by quantitative metallography. Identification was based on optical properties. The fineness and rarity of inclusions excluded extraction followed by electron microprobe analysis as a means of identification.

The concentration of the major alloying element in each alloy was determined by wet chemical analysis. Carbon was evaluated by conductometry.

Gases were analyzed by vacuum fusion technique,inert fusion or vacuum distillation analysis,or even emission spectroscopy,depending on the expected concentration. All minor elements were determined by emission spectrography. Semi-quantitative analysis on the surface of specimens as well as on surfaces of internal macropores was conducted by an energy dispersive X-ray analyzer attached to the scanning electron microscope.

SKYLAB SPECIMEN 1.6

(Released Type Ni-Sn)

I. RESULTS OF SPECIMEN EVALUATION

A. NON-DESTRUCTIVE EVALUATIONS

1. Sphericity

a. Micrometric Examination

The major axis (half diameter), a, of the spheroid is 0.331 $\pm$ 0.005 cm, the minor axis, b, orthogonal to a is 0.312 $\pm$ 0.005 cm and the intermediate axis (mean axis), c, orthogonal to a and b is 0.326 $\pm$ 0.005 cm.

b Shadowgraphic Examination

Top and side projections of shadows are illustrated in Figure 2. Measured axes are: a = 0.370 cm, b = 0.310 cm and c = 0.320 cm.

2. Density

The density, evaluated pycnometrically, was found equal to 7.85 gm/cm^3.

3. Surface Smoothness

Scanning electron micrographs are illustrated in Figure 3. The surface is rough and consists of equiaxed dendrites with substantial interdendritic depressions that can be attributed to solidification shrinkage. At a given location (L) on the surface of the specimen a different type of equiaxed dendrites, that are "two-dimensional" is observed. Such morphologies are reminiscent of dendrites observed on chilled surfaces of ingots. The "two-dimensional" dendrites are illustrated in Figure 3c which also shows some regular equiaxed dendrites at the lower right corner.

These regular equiaxed dendrites are further illustrated in Figure 3d. A morphological peculiarity is observed on the surface of dendrites that outcrop in surface shrinkage cavities: Dendrite arms appear terraced, Figures 4a and b.

B. DESTRUCTIVE EVALUATIONS

1. Grain Formation

Figure 1 illustrates a meridian cross-section of the specimen. The grain structure is columnar (A) at the lower part of the specimen, that was in contact with the ceramic substrate during solidification, and becomes coarse equiaxed (B) at a distance of about 0.1 cm from the substrate. The columnar structure comprised a finer structure (average length 1000 microns and average width 50 microns) and a coarser structure (average length 800 microns and average width 160 microns). The coarse equiaxed structure exhibits an average grain size of 220 microns. Beyond the coarse equiaxed structure the specimen consists of a fine equiaxed grain structure (C) (average grain size 10 microns).

2. Microporosity

Microporosity is readily observed metallographically, Figures 3 and 4. It is basically located close to the surface of the spheroid and assumes the ragged morphology of interdendritic shrinkage micropores, Figure 3. Extensive shrinkage microporosity is also observed across the specimen along the contact between fine and coarse equiaxed grain or dendritic structures, Figure 4d. A perfectly round gas micropore is also observed, Figure 4c.

The total volume percent microporosity calculated from density considerations is: [(8.73-7.85)/8.73] x 100 = 10.08% (8.73 is density of perfectly compact Ni-10.05% Sn and 7.85 is measured density)]. Quantitative metallographic estimation of microporosity gave an average of 9.17% with a maximum of 30.1% near the region where large micropores were observed and a minimum of 0.20% within the columnar structure. Such low amounts microporosity were evaluated by X-ray microradiography. Computerized image analysis gave slightly higher values than did quantitative metallography, probably because some particles of Ni_3Sn might have been mistaken for micropores. Pore size varied between 2 microns (observed by X-ray microradiography) and 900 microns. The shape and size of shrinkage micropores are difficult to define quantitatively, because of their geometrical complexity.

3. Dendritic Structure

The lower part of the specimen next to the ceramic substrate is columnar dendritic (A) with interdendritic nonequilibrium Ni_3Sn. Average secondary dendrite arm spacing is 15 microns. Spacing increases with distance from the ceramic substrate. The columnar structure is followed by a coarse equiaxed dendritic structure (B), Figure 5b, of average secondary dendrite arm spacing equal to 22 microns. Nonequilibrium Ni_3Sn occupies the interdendrite spaces. The fine equiaxed structure (C), Figures 4c and d, and 5a and d is almost nondendritic and it is difficult to define a secondary dendrite arm spacing. Figure 6 illustrates the

geometry of the interdendritic microconstituent that consists of an almost divorced eutectic α-Ni/Ni_3Sn.

4. Secondary Phases, Segregation, Nonmetallic Inclusions.

a. Secondary Interdendritic Phase

The nonequilibrium interdendritic phase was identified by X-ray diffraction analysis as being Ni_3Sn. In microstructure (A) the average volume fraction of Ni_3Sn - established by quantitative metallography - was found to be equal to 0.064, in microstructure (B) equal to about 0.062 and in microstructure (C) equal to 0.055. The same measurements were also conducted by computerized image analysis (M.R. Quantimet 720). Volume fractions were: 0.073, 0.070 and 0.0.070 for microstructures (A), (B) and (C), respectively.

b. Microsegregation

The minimum tin concentration, Cm, found along the axes of secondary dendrite arms, using a focused electron microprobe beam was: 4.3 wt% Sn in microsturctures (A) and (B), and 4.9 wt% Sn in microstructure (C). The maximum tin concentration within the α-primary dendritic phase, C_M, was found to be approximately 15 wt% Sn in all cases.

c. Macrosegregation

The average tin concentrations measured with a defocused electron beam were: 9.85 wt% Sn in microstructure (A), 10.15 wt% Sn in microsturcture (B) and 10.10 wt% Sn in microstructure (C).

d. Nonmetallic Inclusions

Inclusions were rare, very fine and their observation and

identification was difficult. Inclusion sizes were about 0.5-1.5 microns. On the basis of optical properties, silica and probably a spinel were detected. Inclusion extraction and identification by electron microprobe analysis was not attempted, because of the very small amount of material available and the small amount of inclusions as well.

5. Microhardness Survey

Within the nickel-rich dendrite phase the average microhardness was 252 VHN in microstructure (A) and (B), and 265 VHN in microstructure (C) along secondary dendrite arm axes. At dendrite arm boundaries the microhardness was 280 VHN within microstructures (A) and (B), and 285 VHN within microstructure (C). Within Ni_3Sn the average microhardness was about 490 VHN.

6. Chemical Composition

The concentration of tin, determined by wet chemical analysis was found to be 10.05 wt%. The variation of tin concentration with locations within the specimen was given above as macrosegregation.

Analysis of gases, conducted as described in the Introduction was: O: 20 ppm, N: 4 ppm and H: 2 ppm. Other elements analyzed by emission spectrography were: Si: 5 ppm, Mg: 5 ppm, Cr: 5 ppm, Cu: 15 ppm, Zn+Pb: 10 ppm, Ti: 5 ppm, Co: 5 ppm and Fe: 10 ppm. Carbon concentration was about 10 ppm.

II. DISCUSSION OF SOLIDIFICATION BEHAVIOR

This specimen melted completely. Growth started epitaxially on

the ceramic substrate generating the columnar dendrite structure (A). With increasing distance from the ceramic heat sink the thermal gradient in the liquid at the solid-liquid interface (G) decreased faster than did growth rate (R). Below a certain critical value (G/R) the columnar structure broke down with formation of the coarse equiaxed dendritic structure (B). This formation appears to have been assisted by some convection which can be attributed to solidification shrinkage. While structures (A) and (B) grew, loss of heat by radiation cooled down the specimen surface opposite to the ceramic substrate until at certain undercooling surface nucleation took place and propagated into the rest of the melt. Surface nucleation is thought responsible for the two-dimensional dendrites observed in this specimen as well as in the ground specimens of this alloy and of nickel-copper alloy. Growth of the nuclei that formed within the undercooled remaining liquid led to formation of microstructure (C) that consists of very fine "pseudodendritic" grains. The extensive shrinkage micropc osity observed at the contact between regions (C), and (B) or (A), Figure 4d, can be easily justified, since this interstructural zone was occupied by the last liquid to solidify between the growing microstructure (C), and (B) or (A). Because of the absence of gravity the growing grains of microstructure (C) did not "shower" on the advancing microstructures (B) or (A). The absence of gravity, hence of metallostatic pressure is responsible for the spherical shape of the gas micropore, Figure 4c. The basic difference between Skylab and ground-processed Ni-Sn specimens is precisely this undercooled structure.

SKYLAB SPECIMEN 2.8

(Released Type Ni-Ag)

I. RESULTS OF SPECIMEN EVALUATION

A. NON-DESTRUCTIVE EVALUATIONS

1. Sphericity

a. Micrometric Examination

The major, minor and intermediate axes of the spheroid are: $a = 0.380 \pm 0.005$ cm, $b = 0.320 \pm 0.05$ cm and $c = 0.360 \pm 0.005$ cm.

b. Shadowgraphic Examination

Values obtained by using top and side views of the projected shadows are the following: $a = 0.395$ cm, $b = 0.340$ cm and $c = 0.370$ cm.

2. Density

The density evaluated by pycnometry was found equal to 8.80 gm/cm^3.

3. Surface Smoothness

Scanning electron micrographs of the specimen surface are illustrated in Figure 8. A large portion of the specimen did not melt. The resolidified portion exhibits a fairly smooth surface with limited occurrence of solidification shrinkage cavities, but extensive occurrence of patterns that can be attributed to silver evaporation and thermal grooving.

B. DESTRUCTIVE TESTING

1. Grain Formation

The macrostructure illustrated in Figure 1 is that of a meridian cross-section that cuts through the unmelted part of the specimen (A). The resolidified specimen includes a columnar grain struc-

ture (B) with grains of average length = 900 microns and average width = 210 microns, and an equiaxed grain structure (C) with grains of average size = 100 microns. Both grain size measurements are affected by a wide scatter.

2. Microporosity

Metallographic examination showed very limited microporosity. The total volume percent microporosity calcualted from density considerations is: [(9.00-8.80)/9.00] x 100 = 2.22% (9.00 is density of perfectly compact Ni-0.68 st% Ag and 8.80 is measured density). By quantitative metallography the average volume percent microporosity found was 1.85%, with a maximum of 3.15% and a minimum of 0.25%. This low volume percent microporosity was measured by X-ray microradiography.

3. Dendritic Structure

Microstructure (B), Figures 1, ., and 9d is columnar dendritic with secondary dendrite arm spacing of about 25 ns next to the ceramic substrate and up to 40 microns at about 0.2 cm from the substrate. Microstructure (C) is equiaxed dendritic, Figure 9c, with secondary dendrite arm spacing of about 40 microns.

4. Secondary Phases, Segregation, Nonmetallic Inclusions

a. This two-phase monotectic alloy consists in the as-cast condition of primary dendrites of nickel-rich phase with interdendritic discrete particles of a nonequilibrium phase that appears to be almost pure silver. These particles are very fine and are responsible for the formation of etch pits that appear as black spots

delineating the secondary dendrite arm boundaries, Figure 9c. The appropriate way to define microsegregation in this system would have been by indicating the minimum silver concentration, C_m, measure along dendrite arm axes, and/or by the volume percent of nonequilibrium secondary phase (Ag). Measurement of this volume percent appeared impossible to make because of its very low value. Measured value of C_m = 0.55 wt% Ag. At dendrite arm boundaries, away form silver particles, a maximum C_M = 0.85 wt% Ag was measured.

c. Macrosegregation

The average silver concentration measured with a defocused electron beam was 0.64 wt% in microstructure (B) and 0.72 wt% in microstructure (C).

d. Nonmetallic Inclusions

Silica, silicoaluminate and sulfide particles of very fine sizes (about 1 micron) and in extremely small quantities were detected. It appeared impossible to make any volume percent measurements.

5. Microhardness Survey

An average microhardness of 125 VHN was measured within the resolidified part of the specimen. Measurements were made with both microstructures (B) and (C) and exhibited very narrow scatter.

6. Chemical Composition

The silver concentration, determined by chemical analysis was found to be equal to 0.68 wt%. Elements analyzed by techniques

summarized in the Introduction were: Mg: 5 ppm, Si: 5 ppm, Cu: 15 ppm, Zn + Pb: 15 ppm, O: 15 ppm, N: 5 ppm.

II. DISCUSSION OF SOLIDIFICATION BEHAVIOR

This specimen melted partially. The unmelted part (A) recrystallized due to the heat released by the adjacent solidifying melt. This melt solidified in a coarse dendrite fashion that is equiaxed, with columnar tendencies near the unmelted material or towards the ceramic substrate. Growth was epitaxial and the liquid did not undercool. The specimen lost a significant amount of its silver by vaporization. The minute silver particles that appear interdendritically and are manifested by etch-pits are the result of a monotectic reaction late during the solidification process. There is no evidence of any effect of zero-gravity environment on the microstructure or solidification behavior of this specimen. No meaningful qualitative or quantitative difference was established between this specimen and the ground-processed Ni-Ag alloy.

SKYLAB SPECIMEN 2.4

(Retained Type Ni-Ag)

I. RESULTS OF SPECIMEN EVALUATION

A. NON-DESTRUCTIVE EVALUATIONS

1. Sphericity

a. Micrometric Examination

The specimen is perfectly spherical with radius equal to 0.275 ± 0.005 cm.

b. Shadowgraphic Examination

Using top and side shadow projections the radius was found equal to 0.290 cm.

2. Density

The density, evaluated pycnometrically was 8.90 gm/cm^3.

3. Surface Smoothness

Figure 11 exhibits scanning electron micrographs of the specimen surface. The surface is extremely smooth with only a few grain boundaries that are not grooved. No dendritic pattern is seen on the surface, presumably because the specimen has lost a lot of its silver. The absence of surface dendrites, hence of inter-dendritic solidification shrinkage is thought to be partly responsible for the surface smoothness.

B. DESTRUCTIVE EVALUATIONS

1. Grain Formation

A meridian cross-section of the specimen is illustrated in Figure 1. Grain size is very coarse, approximately 1010 microns,

Figure 12c. The surface layer comprises only five grains. All grains are equiaxed dendritic and there is evidence that secondary grain growth has taken place.

2. Microporosity

The amount of microporosity within the specimen is extremely limited. From density considerations the volume percent microporosity is: $[(8.99-8.90)/8.99] \times 100 = 1.01\%$. (8.99 is density of perfectly compact Ni-0.57 wt% Ag and 8.90 is measured density). X-ray microradiography has confirmed an extremely low amount of micropores that are submicron in size.

3. Dendritic Structure

The specimen is coarse dendritic, consisting of dendrite "cells" of the primary nickel-rich phase, analogous to those observed in very slowly cooled alloys. Such dendrite "cells" of average size equal to 190 microns may be attributed to extensive coarsening and coalescence that take place during solidification. The interdendritic spaces appear to be richer in silver with locally recognizable silver particles, Figures 12b and d. Figure 12c indicates clearly that extensive grain growth has taken place after completion of solidification. Such growth could not be prevented by the very low amount of silver particles present at dendrite "cell" boundaries.

4. Secondary Phases, Segregation, Nonmetallic Inclusions

a. Some particles of secondary phase (Ag) have been observed along dendrite "cell" boundaries. The specimen appears to have lost, at least close to the surface, an appreciable amount of silver

by vaporization from the melt.

b. Microsegregation

Within the dendrite "cells" no significant variation of silver concentration was detected. On the average, the concentration was 0.49 wt% Ag.

c. Macrosegregation

The average concentration of silver measured at various locations within the spherical specimen, using a defocused electron beam appeared to be constant and equal to 0.52 wt%.

d. Nonmetallic Inclusions

Some very rare and fine inclusions were identified as silica, sulfides and silicoaluminates. No size or volume percent measurements have been possible to make.

5. Microhardenss Survey

Very minor differences in microhardness were found between different locations within the specimen. An average microhardness of 115 VHN was measured.

6. Chemical Composition

The silver concentration, determined by wet chemical analysis, was found to be equal to 0.57 wt%. Other elements present were: [Mg: 3 ppm, Si: 3 ppm, Cu: 10 ppm, Zn + Pb: 10 ppm, O: 20 ppm, N: 20 ppm].

II. DISCUSSION OF SOLIDIFICATION BEHAVIOR

The specimen melted completely and assumed a perfectly spherical shape. Solidification was dendritic with spacings of about 190 microns, that is about 5 times coarser than those observed in

the SL-2.8. The reason for this very slow solidification is that this specimen was heated for about 25 seconds,hence superheated much more than the SL-2.8 specimen or the ground-processed specimens #1-4 and #1-11 which were heated for a shorter time(e.g. specimen SL-2.8 was heated for 15 seconds) and cooled down slower. Slow solidification is responsible for the extensive coarsening and coalescence that led to formation of coarse "dendrite cells" (average "cell" size=190 microns,as opposed to dendrite arm spacing in ground-specimen #1-4 equal to 25-35 microns). The specimen has lost a substantial fraction of its silver content during this long heating(0.57wt%Ag in SL-2.4 and 0.85wt%Ag in ground-specimen # 1-4).Extensive grain growth took place because of slow cooling of the solid and high purity (grain size= 1010 microns in SL-2.4 and only 305 microns in ground-specimen # 1-4). Some coarse silver particles that formed monotectically were detected between dendrite cells. Microhardness in SL-2.4 was on the average=115 VHN, as compared with that in ground-specimen # 1-4,equal to 138VHN. This property should be correlated with the amount of silver within the specimen.The extreme smoothness of the SL-2.4 specimen may be attributed to the very small number of grain boundaries that uotcrop on the surface,and to the absecence of surface dendrites or interdendritic shrinkage.

SKYLAB SPECIMEN 1.10

(Released Type Pure Ni)

I. RESULTS OF SPECIMEN EVALUATION

A. NON-DESTRUCTIVE EVALUATIONS

1. Sphericity

a. Micrometric Examination

The major, minor and intermediate axes of the specimen are: a = 0.320 cm, b = 0.285 cm and c = 0.310 cm. An error of $\pm$ 0.005 cm affects these measurements.

b. Shadowgraphic Examination

Using top and side shadow projections the following values were obtained: a = 0.343 cm, b = 0.293 cm and c = 0.327 cm.

2. Density

The density, evaluated pycnometrically, was found equal to 8.65 gm/cm^3.

3. Surface Smoothness

Figures 13 and 14 illustrates the surface morphology of the specimen. Outcropping macroporosity can be seen in Figure 13a, and surface patterns probably caused by flow and vaporization can be seen in Figures 13b, c and Figure 14. The contact between melted and unmelted specimen is characterized by a deep gap that is seen in Figure 13d.

B. DESTRUCTIVE EVALUATIONS

1. Grain Formations

The cross-section of the specimen, Figure 1, illustrates the part

that did not melt (A) and the part that melted and resolidified (B). Average grain size in microstructure (A) is 100 microns and in microstructure (B) 1000 microns.

2. Microporosity

Some microporosity is observed on the surface, Figure 13a, and almost no porosity is observed within the specimen. From density measurements the total percent microporosity was found equal to: [(8.99-8.65)/8.99] x 100 = 3.78%. (8.99 is density of perfectly compact nickel and 8.65 in measured density). Quantitative metallographic and X-ray microradiographic analyses gave a volume percent of about 1.75%.

3. Dendrite Structure

No definite dendritic structure was observed in this as-cast pure nickel specimen. When heavily etched and examined under polarized light, the specimen exhibited grains that contained a regular dendrite-like segregation pattern, Figures 15b and c. These patterns may be attributed to impurity segregation.

4. Secondary Phases, Segregation, Nonmetallic Inclusions

No secondary phase, microsegregation or macrosegregation were detected or measured in this specimen. Some silica, silicoaluminate and sulfide inclusions were identified without certainty because of their extreme fineness.

5. Microhardness Survey

The average microhardness was measured and found to be equal to 1.55 VHN. This value was the same for the bulk of the grains.

as well as for grain boundaries.

6. Chemical Composition

Elements analyzed using techniques summarized in the Introduction are: O: 10 ppm, N: 5 ppm, H: 2 ppm, Fe: 4 ppm, Cr = 5 ppm, Co = 5 ppm, Si: 5 ppm, Cu: 10 ppm .

II. DISCUSSION OF SOLIDIFICATION BEHAVIOR

The specimen melted partially and resolidified epitaxially on the remaining unmelted solid. Some typical shrinkage microporosity appears on the surface, especially at the boundary between resolidified and unmelted parts, Figure 13d. Ripplemarks appearing on the surface, Figure 13, may be attributed to limited displacement of mushy liquid. Cellular patterns, Figure 14, may be attributed to surface vaporization along boundaries of dendrite cells that might have grown at some locations of the surface. Extensive grain growth after completion of solidification, favored by the purity of the material, should be held responsible for the large grain size observed. The weak dendritic segregation pattern revealed by heavy etchings and examination of the specimen under polarized light may be attributed to impurities. The solidification of this specimen is similar to that of the ground pure nickel specimens, with the exception of the ripple marks that appear only in the Skylab Specimen. There is no evidence of undercooling. No significant difference was established between the microstructure of this specimen and that of ground-processed pure nickel.

SKYLAB SPECIMEN 1.11

(Released Type Pure Ni)

I. RESULTS OF SPECIMEN EVALUATIONS

A. NON-DESTRUCTIVE EVALUATIONS

1. Sphericity

Only a small fraction of the specimen melted and resolidified. It was, therefore, judged unimportant to make any measurements of sphericity.

2. Density

The density of this specimen, evaluated by pycnometry, was found equal to 8.95 gm/cm^3.

3. Surface Smoothness

The surface morphology is illustrated by the scanning electron micrographs of Figure 16. There is no evidence of extensive porosity. Locally, in a shallow shrinkage cavity there is evidence of surface dendritic growth, Figure 16d. The pattern shown in Figure 16c appears to be an ensemble of ripple-marks caused by limited displacement of mushy metal. This displacement appears to have been guided by the machining lines on the underlying unmelted part of the specimen.

B. DESTRUCTIVE EVALUATIONS

1. Grain Formation

The cross-section of Figure 1 exhibits the unmelted microstructure (A) and microstructure (B) that resulted from resolidification. Microstructure (A) consists of equiaxed grains of average size equal to 115 microns. Microstructure (B) consists of coarse equi-

axed grains of average size equal to 327 microns. These grains are heavily twinned, Figure 17, and are randomly oriented with respect to each other.

2. Microporosity

The volume percent microporosity deduced form density measurements is: [(8.99-8.95)/8.99] x 100 = 0.44% (8.99 is density of perfectly compact nickel and 8.95 is measured density) Micropores are very fine. Measurement of the volume percent microporosity by X-ray microradiography gave 0.25%.

3. Dendritic Structure

The dendrite structure that appeared in certain locations on the surface, Figure 16d, did not appear in the bulk specimen. However, very heavy etching and examination of the cross-section in polarized light revealed very vaguely a dendrite-like segregation pattern, Figure 17b. The surface denrites are extremely fine (secondary dendrite arm spacing of about 5 microns).

4. Secondary Phases, Segregation, Nonmetallic Inclusions

No secondary phase, microsegregation or macrosegregation were observed in this pure system. Nonmetallic inclusions were similar to those observed in specimen SL-1.10.

5. Microhardness Survey

An average microhardness of about 150 VHN was found both in the bulk of the grains and at grain boundaries.

6. Chemical Composition

Concentrations of analyzed elements are: [Cu: 3 ppm, Si: 5 ppm, Cr: 5 ppm, Fe: 5 ppm, Co: 3 ppm, O: 15 ppm, N: 3 ppm, H: 2 ppm] .

II. DISCUSSION OF SOLIDIFICATION BEHAVIOR

The microstructure and solidification behavior of this specimen is very similar to that of specimen SL-1.10. Both melted partially and in both the solid grew epitaxially on the unmelted specimen. The observed weak dendritic segregation pattern exhibits equally fine spacing in both cases. The surface dendritic pattern observes in a shallow solidification cavity in this specimen may be attributed to impurity segregation or could be of thermal origin. Such patterns were observed in pure nickel ground specimens too. Ripple-marks appearing on the surface may be attributed to limited displacement of mushy metal; this displacement appears to have been guided by the machining lines on the underlying unmelted specimen. Some of the surface relief could be attributed to impurity vaporization. The specimen did not undercool. No meaningful difference was detected between this specimen and the ground-processed pure nickel.

GENERAL DISCUSSION

The general aim of the Sphere Forming Skylab Experiment was to study the solidification behavior of metals in zero-gravity environment. It was reasonably expected that solidification of released specimens would be containerless-leading to substantial undercooling of the four alloys specifically selected for this purpose-and convectionless-minimizing macrosegregation. A synthesis of results obtained from the five specimens studied is presented below with a discussion focused on these expectations.

I. SPECIMEN UNDERCOOLING

The Ni-Sn specimen SL-1.6 melted completely and nucleated on the ceramic substrate with formation of columnar dendritic structure (A) that grew with decreasing temperature of the remaining melt. A second nucleation phenomenon occurred on the surface of the sphere,because substantial local undercooling of the melt. Microstructure (C) was thus generated. The morphology of this microstructure indicates an undercooling of about 70-100^{o}C. No high solute cores are observed,presumably because they were levelled-off by solid state diffusion accompanying slow cooling of the sphere. It appears certain that had this specimen floated away from the crystalline substrate,it would have undercooled substantially. The Ni-Ag specimen SL-2.8 melted partially with the melt nucleating epitaxially on the unmelted material and in the ceramic substrate. No undercooling is observed. The Ni-Ag retained specimen SL-2.4 melted completely and nucleated against the unmelted sting at very low undercooling. Finally, the pure nickel specimens SL-1.10 and SL-1.11 melted only partially

and the melt nucleated epitaxially on the unmelted material.

None of the five specimens undercooled properly,if at all. However, there are strong microstructural indications that had the specimens melted completely and taken off the substrate,or had the specimens melted completely against an amorphous substrate-as suggested by the author-substantial undercooling would have taken place.

II. CONVECTION IN THE MELT

It is known that convection in the melt is respon[illegible] for "crystal multiplication". In specimens such as these convection may be caused by density differences within the melt or by solidification shrinkage. This second type of convection cannot be eliminated,is very significant and is responsible for certain types of macrosegregation. By examination of microstructures of the solidified specimen it is not possible to decide which type of convection is responsible for which effect. Examination of macrosegregation has not revealed any significant amount. It should be remembered that with the selected alloys no gravity segregation can be observed because of the small difference in densities of Ni,Sn,Ag and Cu. The Ni-Al alloy that was recommended for clarifying this point was not finally selected,because of aluminum vaporization problems.

The specimens studied herein do not allow any estimation of the extent of convection in the liquid. However,in specimen SL-1.8 it can be seen that a big gas micropore is spherical and was entrapped in the bulk of the specimen. The geometry of this micropore indicates that it grew slowly and was not affected by metallostatic pressure. Since it growth was slow,it would have

had the time to float if a gravity field was present. These observations would then indicate reduced gravity.

III. MELT PURIFICATION

Comparison of analyses of Skylab specimens and of the original master alloys indicates losses of tin and silver. It also indicates a certain loss of impurities by vaporization.

A general conclusion to be formulated is that this experiment did not satisfy all expectations but has indicated that expectations could be satisfied. It did not solve the problems involved in solidification processing in space, but has pointed out which these problems are and how they can be faced in future experiments.

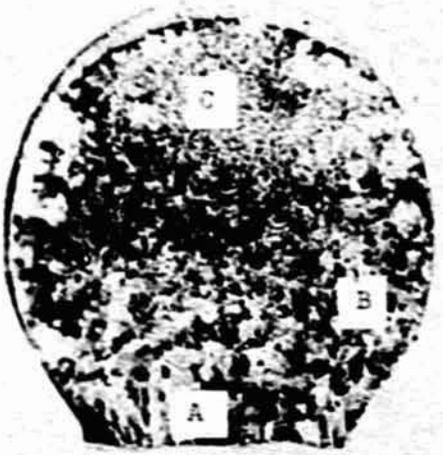

SPECIMEN SL-1.6

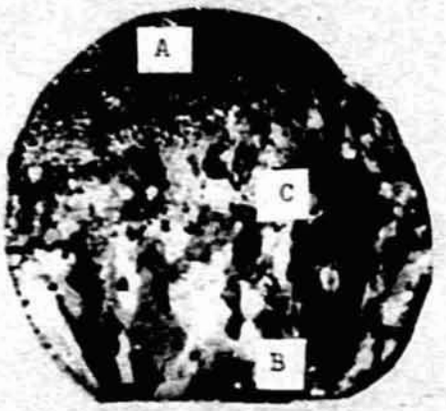

SPECIMEN SL-2.8

SPECIMEN SL-2.4

SPECIMEN SL-1.10

SPECIMEN SL-1.11

Figure 1: Photomicrographs illustrating the macrostructure of Skylab specimens, 10X.

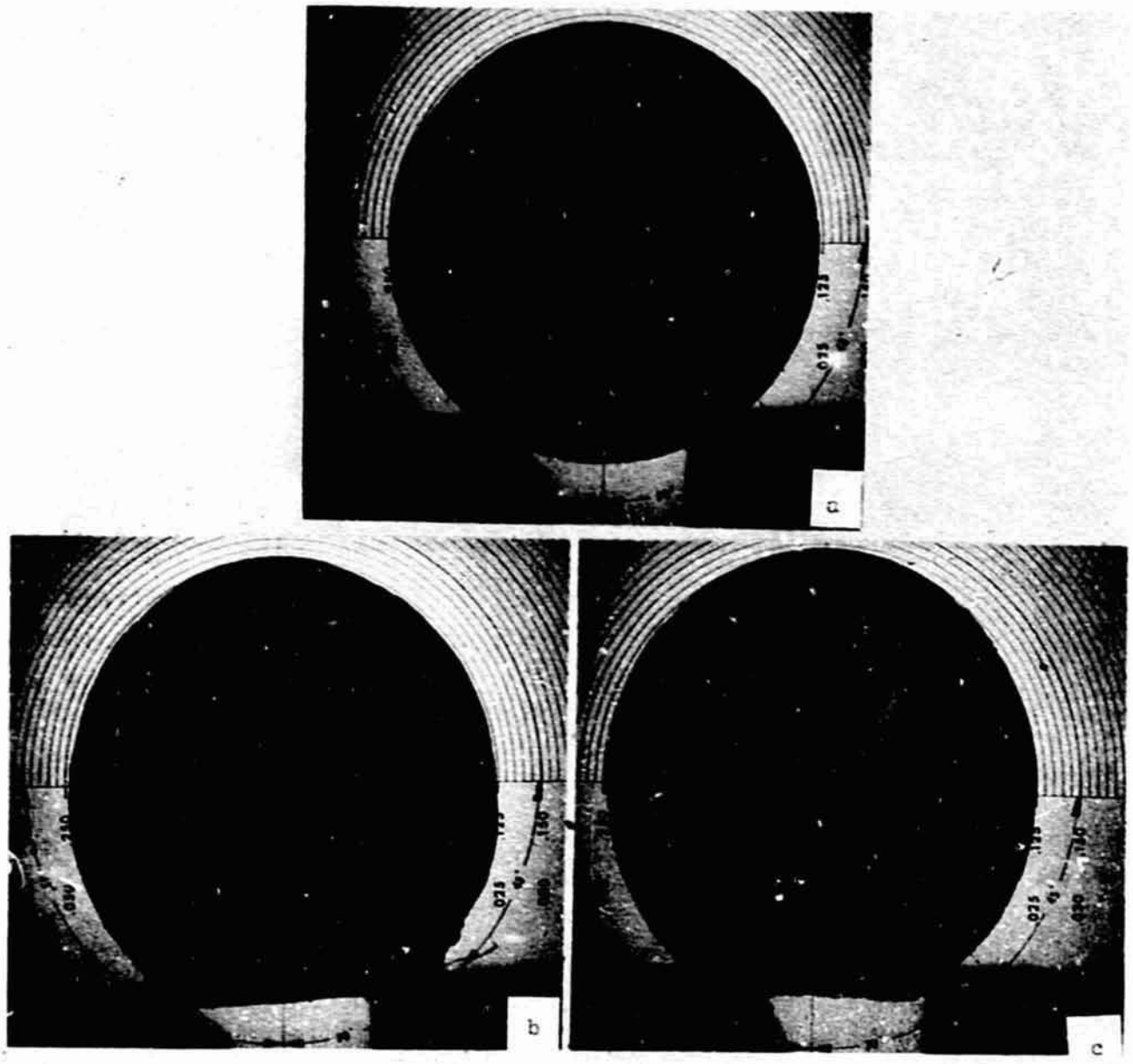

Figure 2: Shadowgraphs of specimen SL-1.6. (a) Top view,(b) and (c) side views,10X.

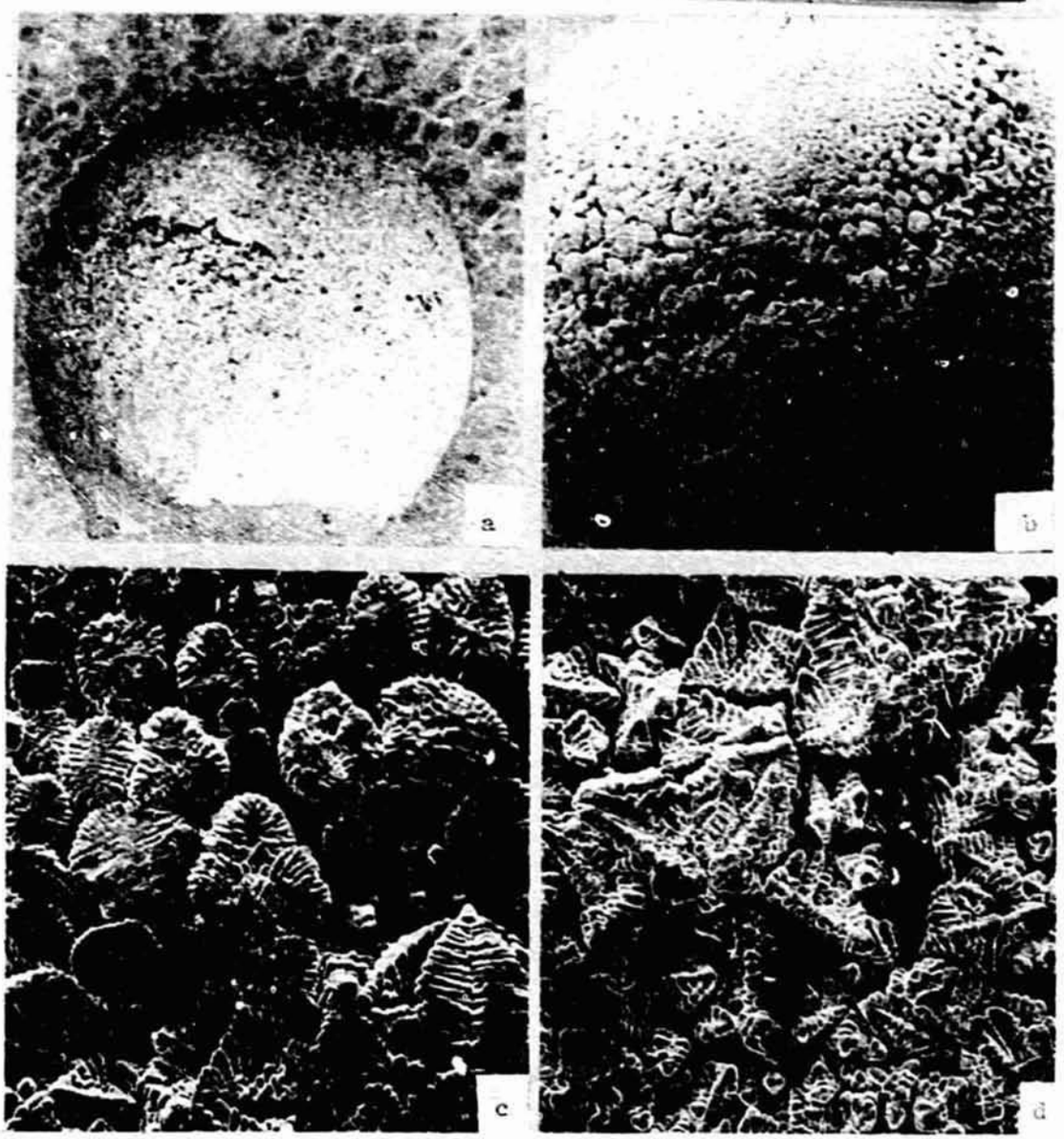

Figure 3: Scanning electron micrographs of surface of specimen SL-1.6. (a) 10X,(b) 25X,(c) and (d) 100X.

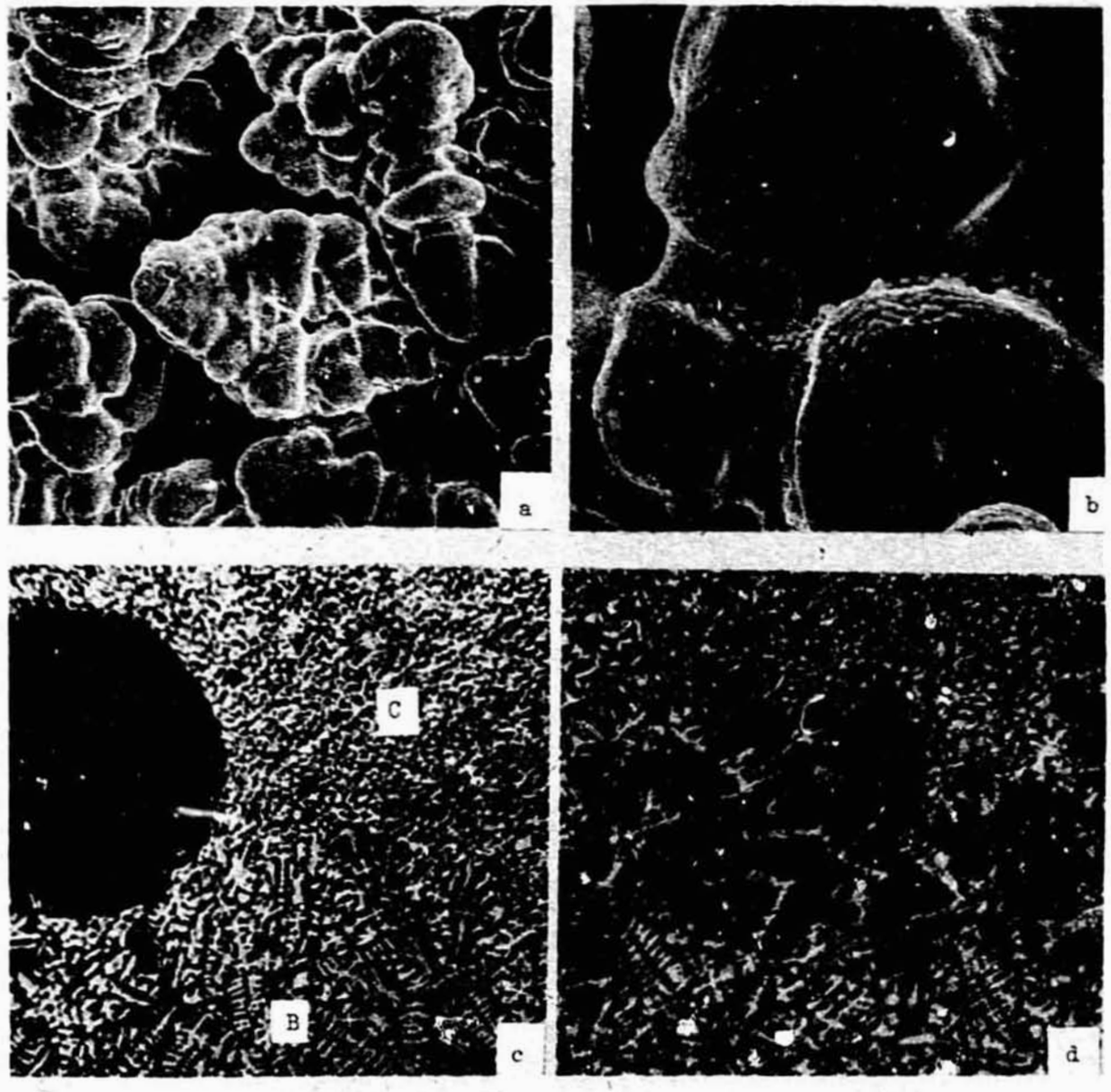

Figure 4: Scanning electron micrographs of specimen SL-1.6.(a) 500X, (b) 2000X. Photomicrographs of specimen SL-1.6 etched with Rosenhain's reagent. (c) and (d) 50X.

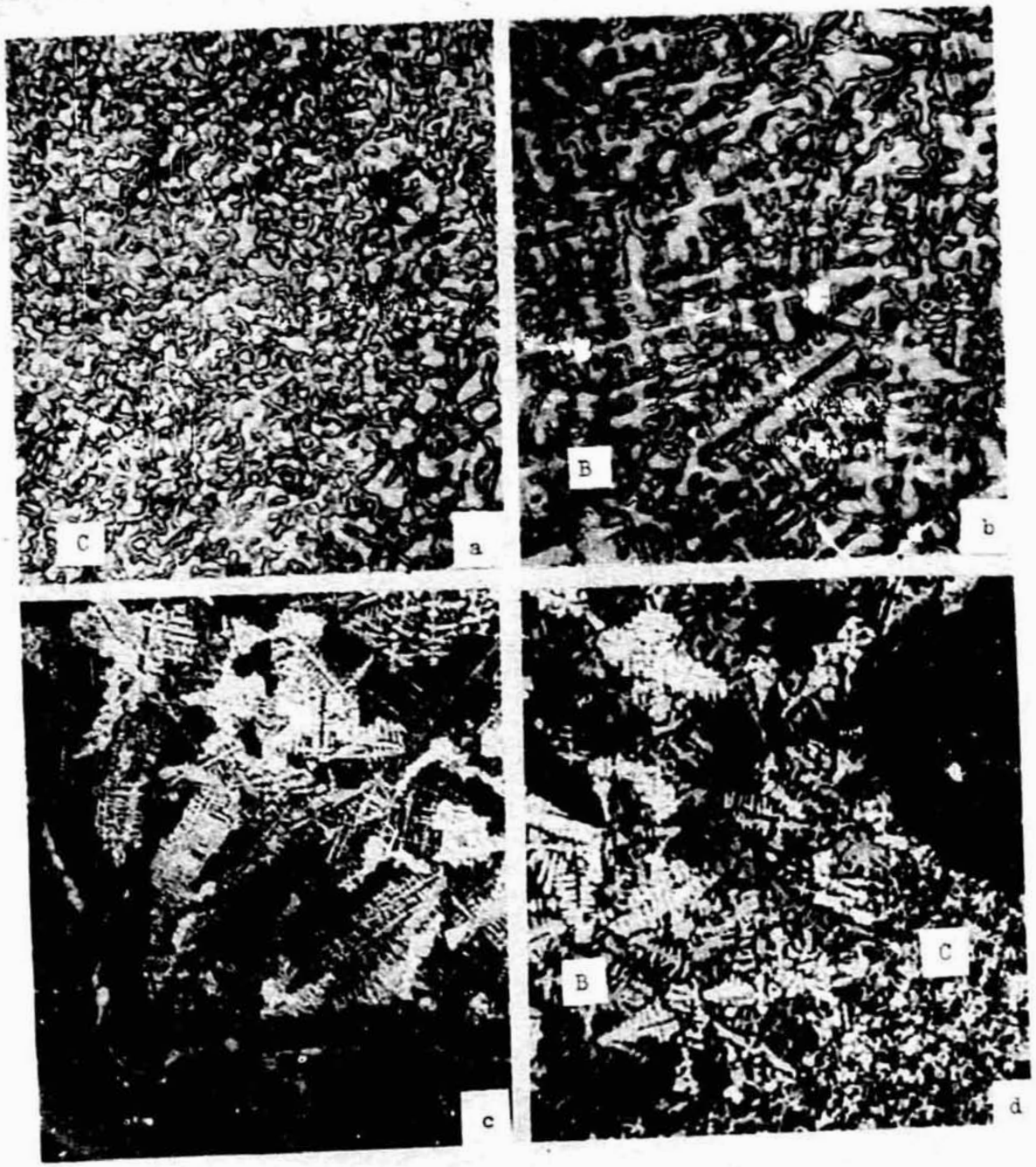

Figure 5: Photomicrographs of specimen SL-1.6 etched with Rosenhain's reagent. (a) and (b) 100X;(c) and (d) polarized light, 50X.

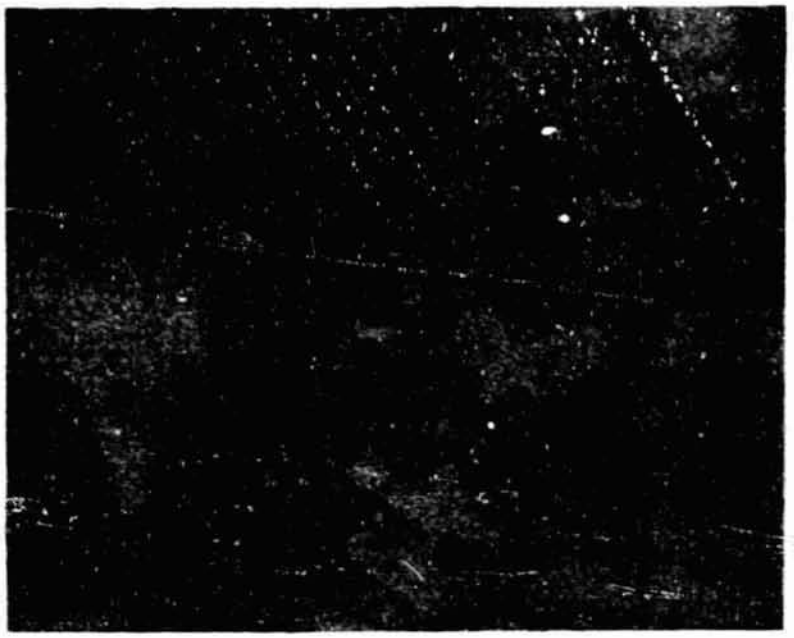

Figure 6: Photomicrograph of specimen SL-1.6 etched with Roserhain's reagent,500X.

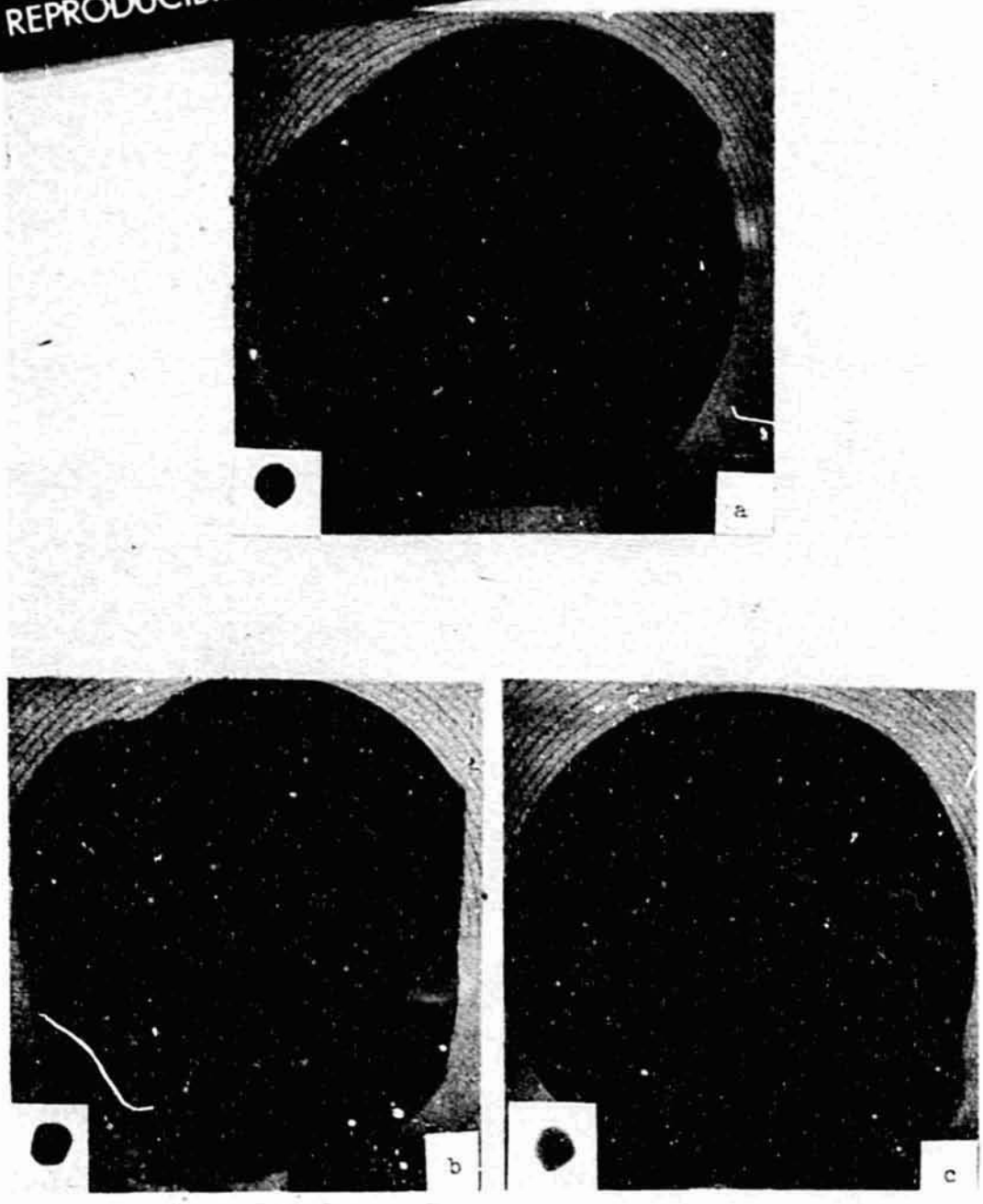

Figure 7: Shadowgraphs (10X) and X-ray macroradiographs (1X) of specimen SL-2.8. (a) Top views,(b) and (c) side views.

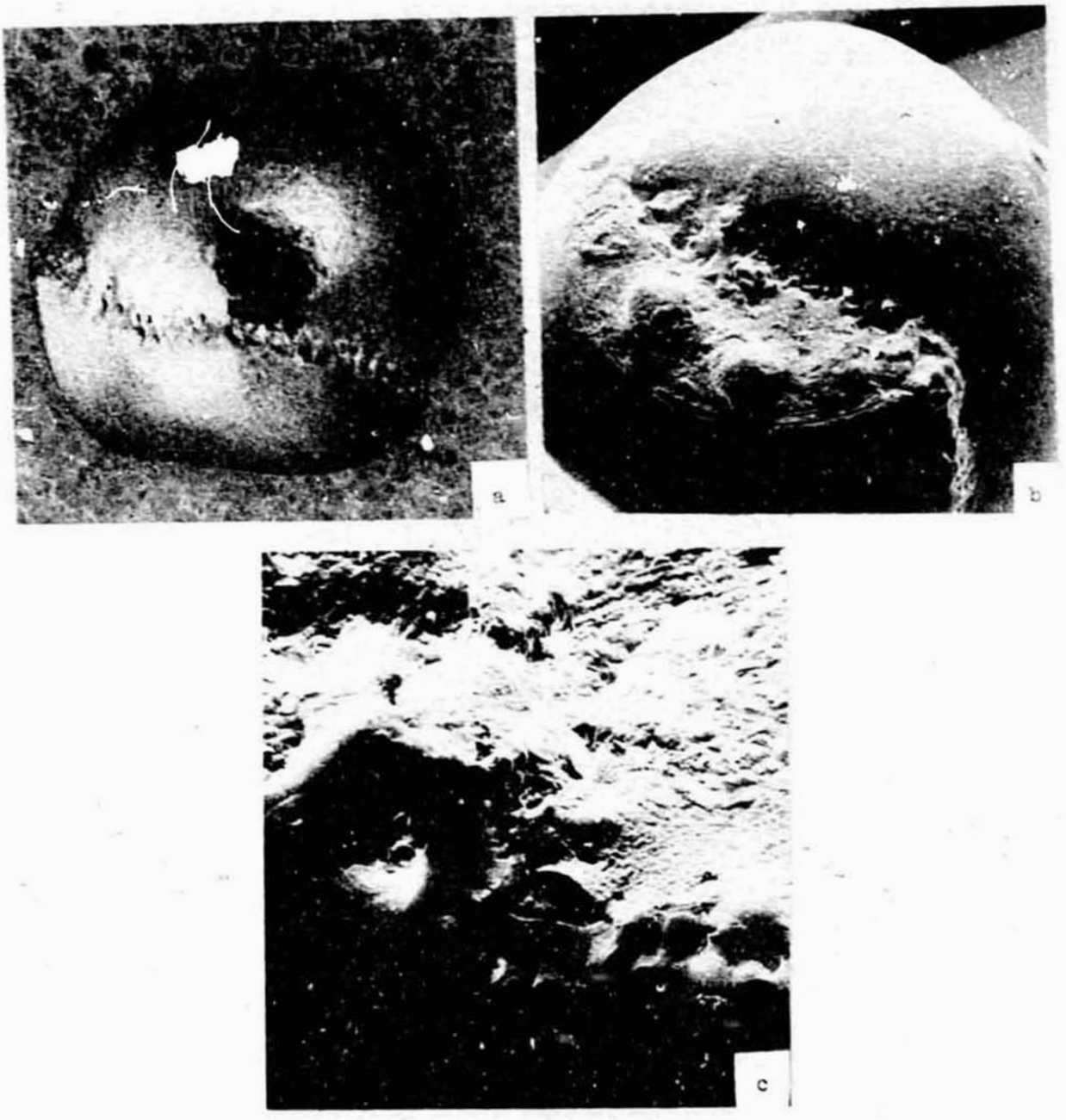

Figure 8: Scanning electron micrographs of specimen SL-2.8. (a) 10X, (b) 25X and (c) 100X.

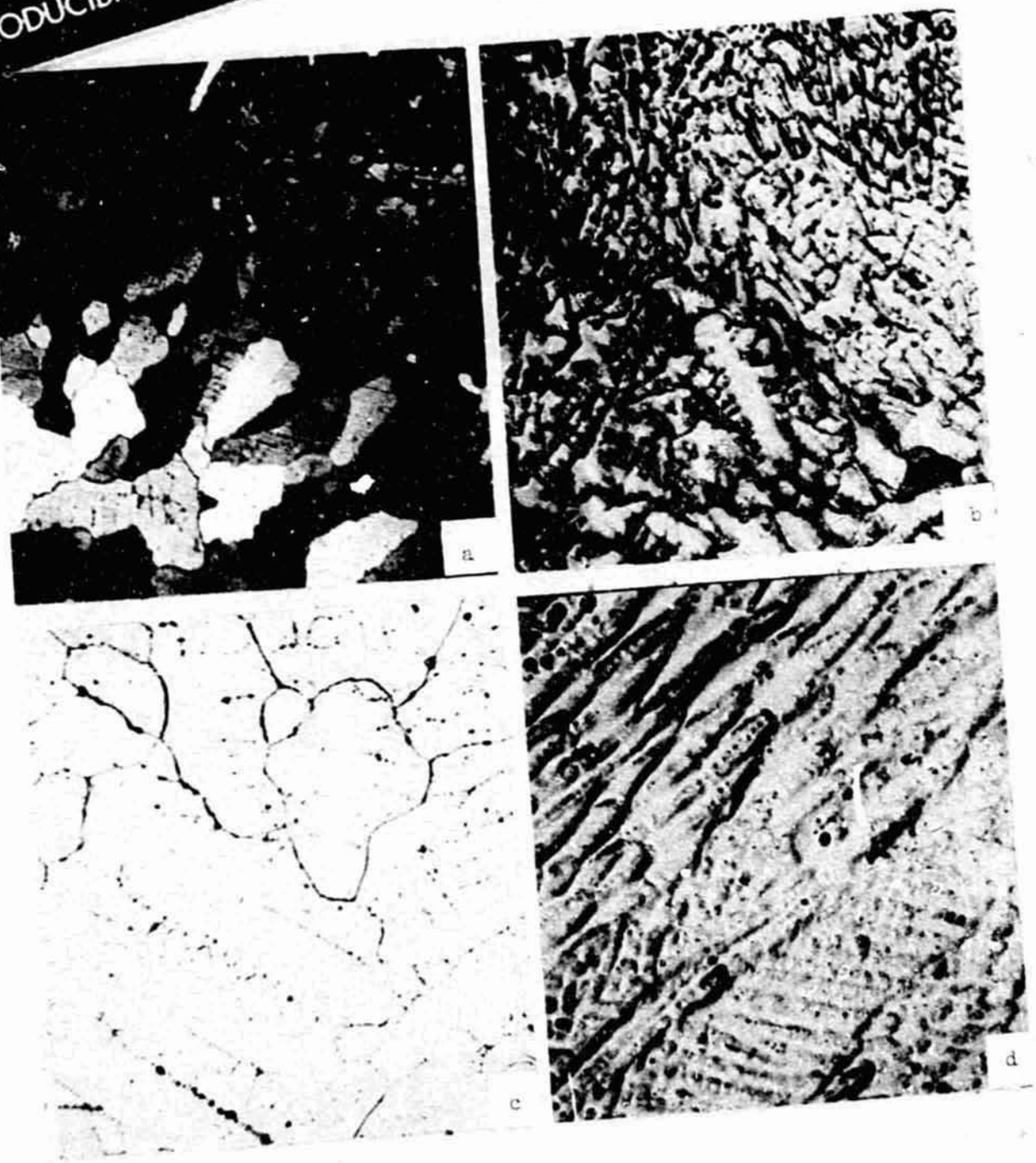

Figure 9: Photomicrograph. of specimen SL-2.8. (a) Polarized light, 100X,(b) 50X,(c) and (d) 100X.

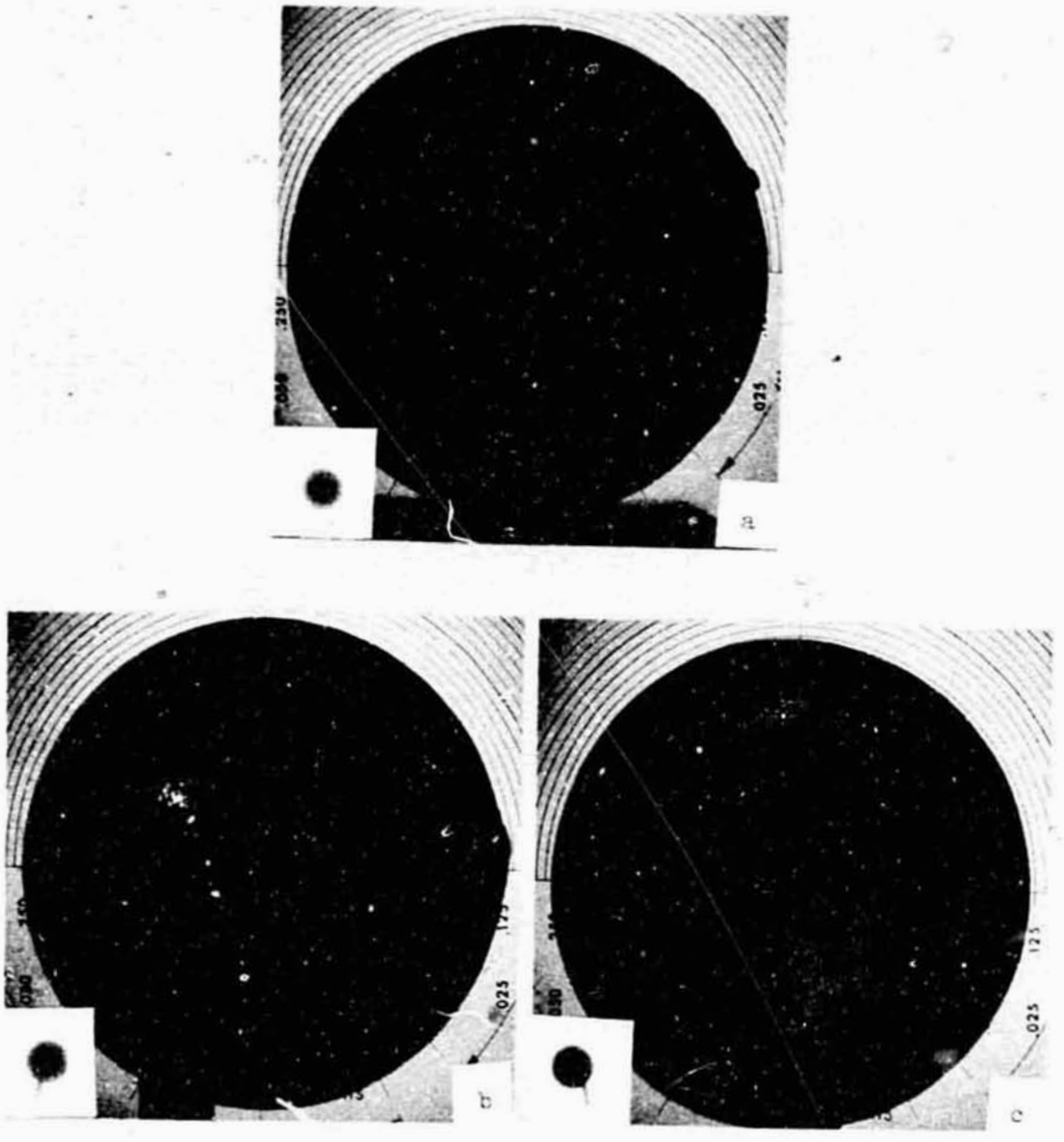

Figure 10: Shadowgraphs (10X) and X-ray macroradiographs (1X) of specimen SL-2.4. (a) Top views,(b) and (c) side views.

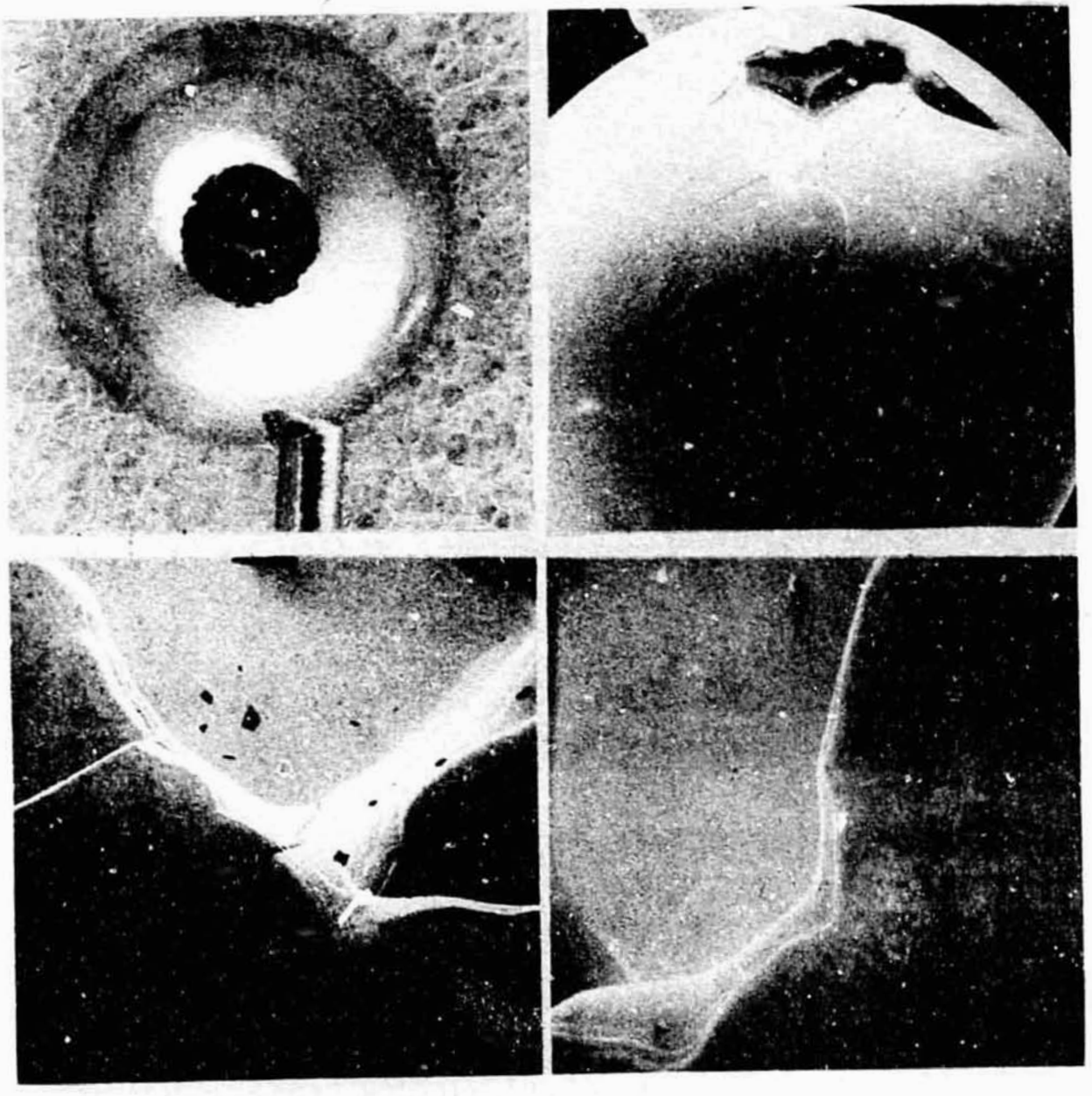

Figure 11: Scanning electron micrographs of specimen SL-2.4. (a) 10X, (b) 25X,(c) and (d) 100X.

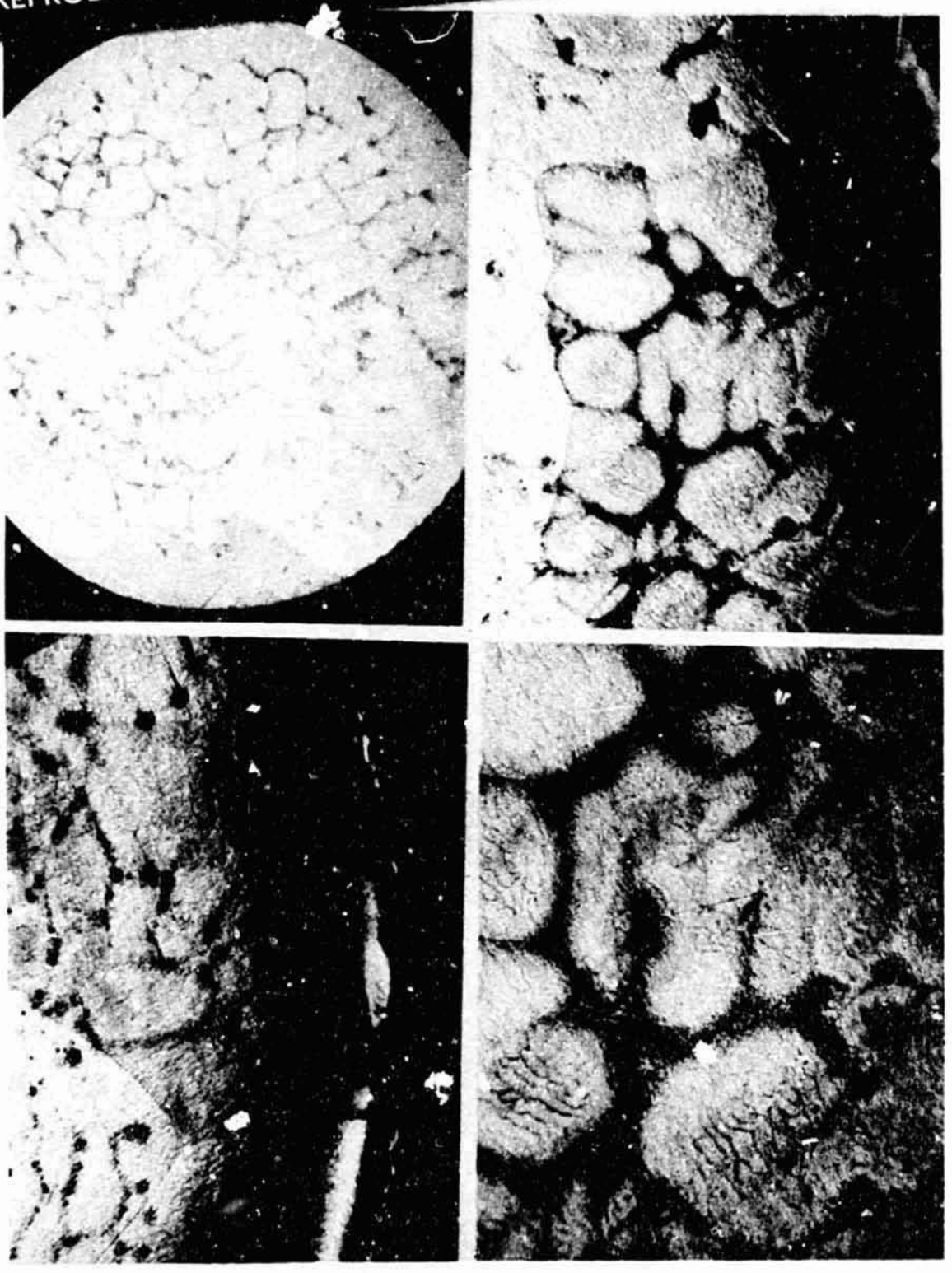

Figure 12: Photomicrographs of specimen SL-2.4 etched with Rosenhain's reagent. (a) 25X,(b) and (c) 50X and (d) 100X.

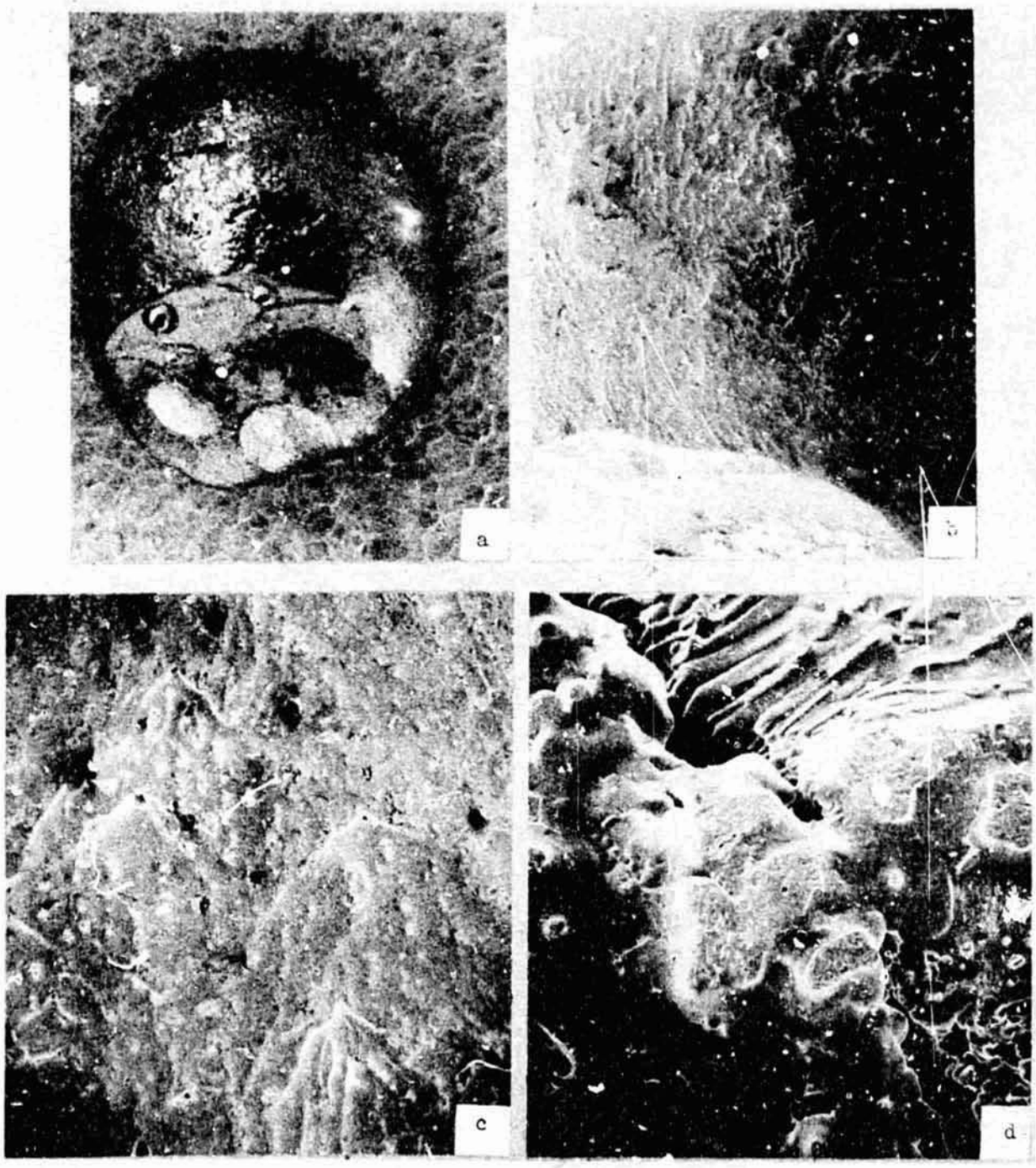

Figure 13: Scanning electron micrographs of specimen SL-1.10. (a) 10X, (b) 25X,(c) 100X and (d) 125X.

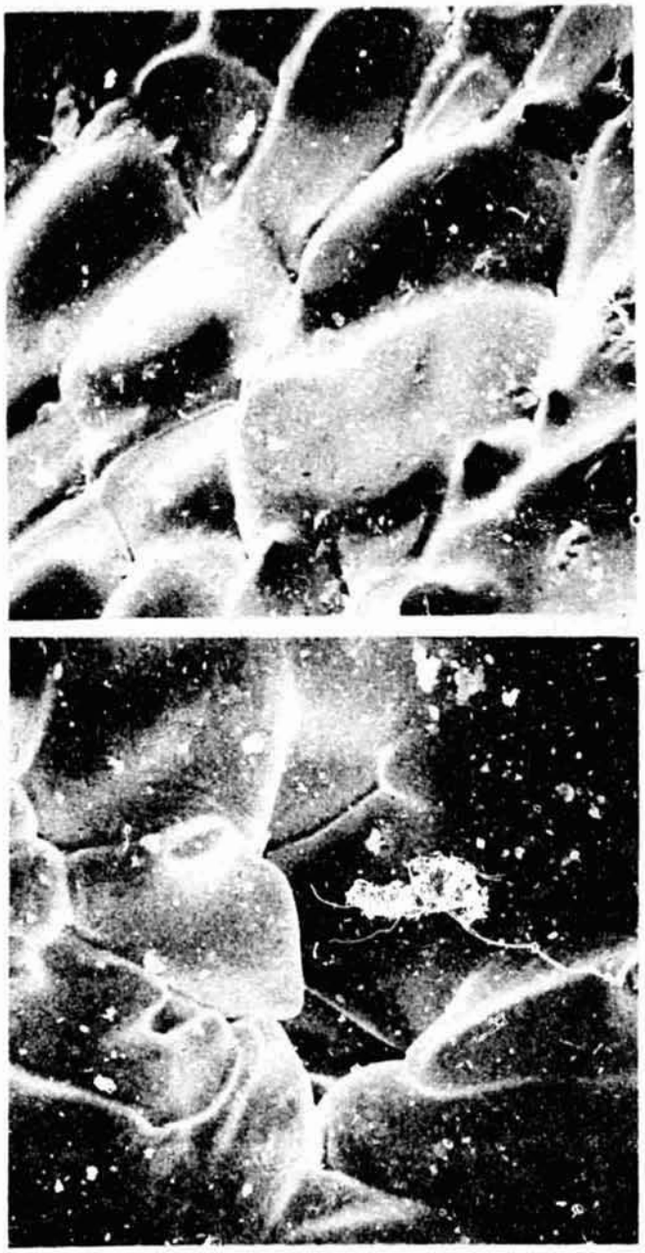

Figure 14: Scanning electron micrographs of specimen SL-1.10,600X.

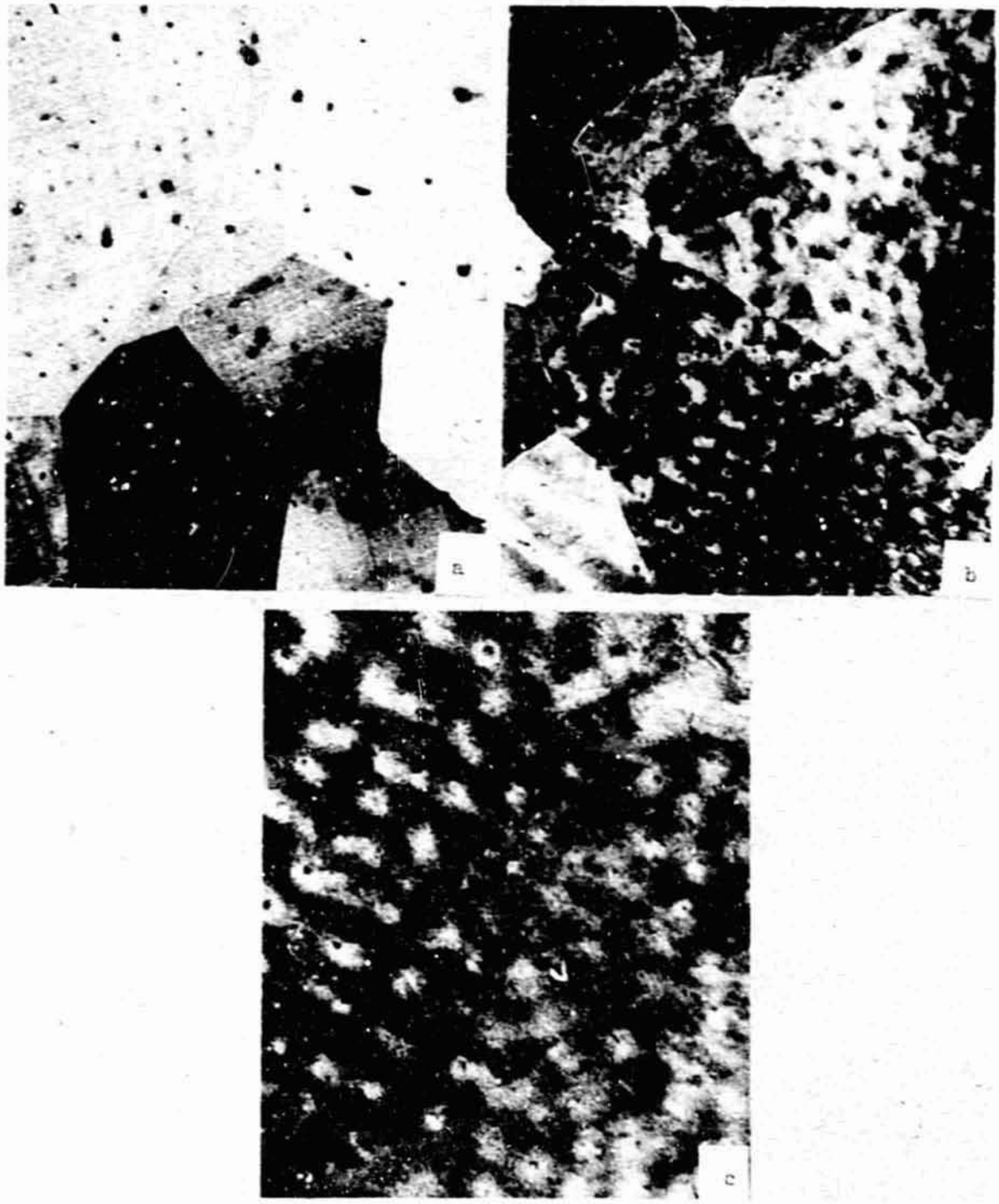

Figure 15: Photomicrographs of specimen SL-1.10, etched with Rosenhain's reagent. Polarized light. (a) and (b) 50X, and (c) 100X.

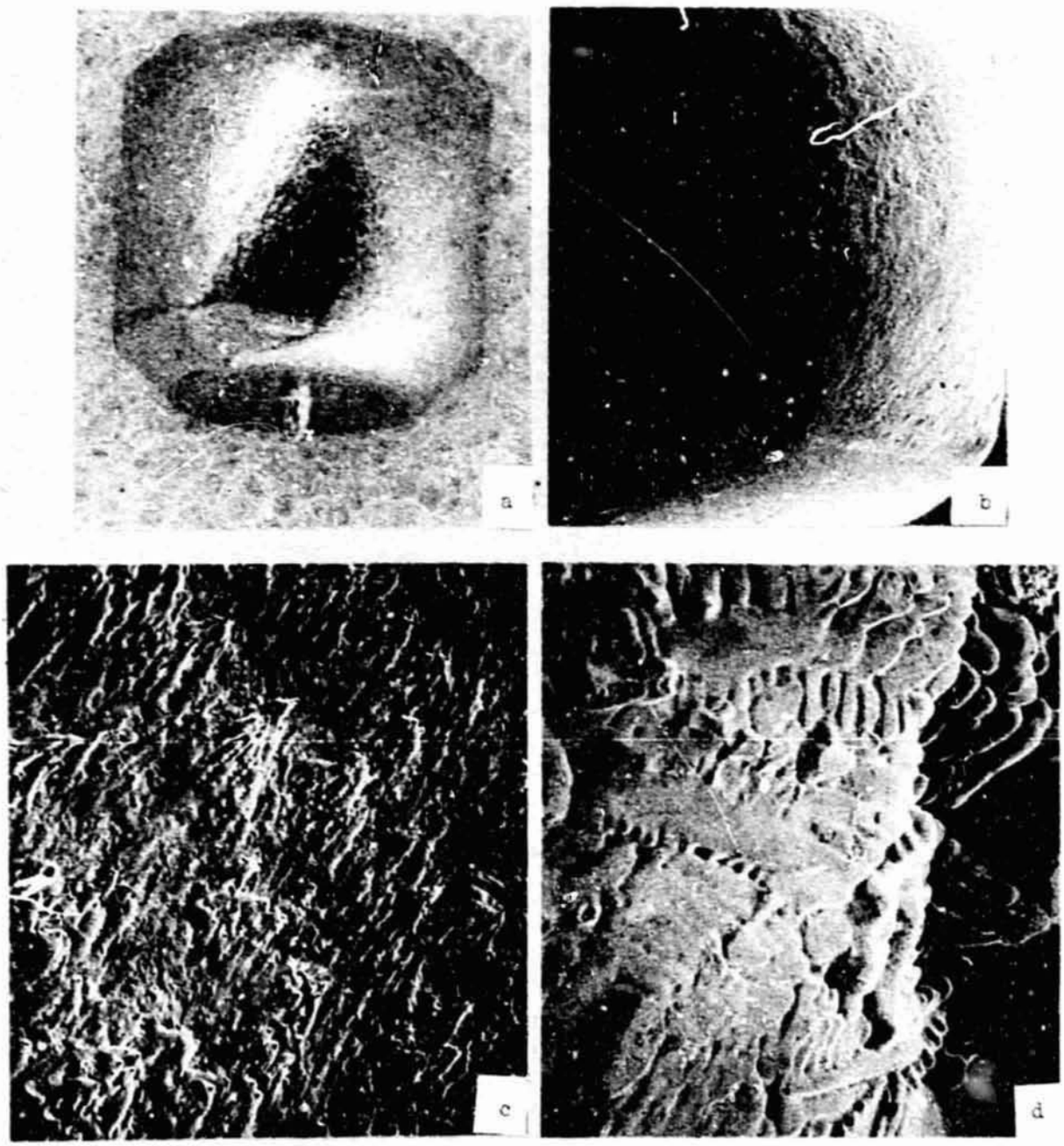

Figure 16: Scanning electron micrographs of specimen SL-1.11. (a) 10X, (b) 25X,(c) 100X,and (d) 500X.

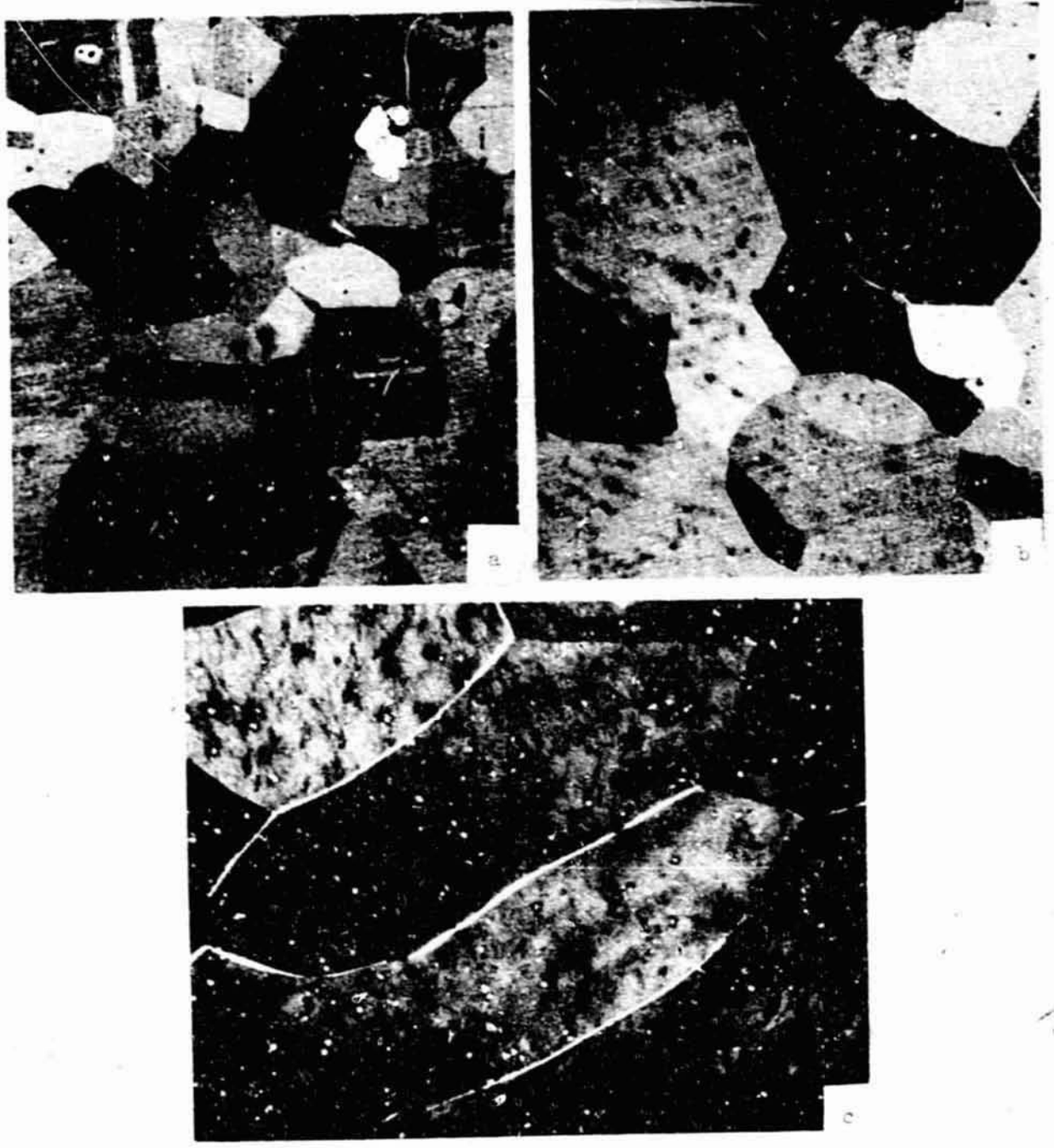

Figure 17: Photomicrographs of specimen SI-1.11,etched with Rosenhain's reagent. Polarized light. (a) and (b) 50X,(c) 100X.